THE NUCLEAR THOMAS–FERMI MODEL WITH ANGULAR MOMENTUM: FISSION BARRIERS, SUPERDEFORMATIONS, MOMENTS OF INERTIA *

W.D. MYERS AND W.J. ŚWIĄTECKI

Nuclear Science Division
Ernest Orlando Lawrence Berkeley National Laboratory
University of California, Berkeley, California 94720, USA

(Received December 10, 1996)

We added a rotational energy to our Thomas–Fermi nuclear model of W.D. Myers, W.J. Świątecki, *Acta Phys. Pol.* **B27**, 99 (1996) and W.D. Myers, W.J. Świątecki, *Nucl. Phys.* **A601**, 141 (1996) and present here a survey of fission barriers, deformation energies, γ-ray rotational cascades and moments of inertia. We explore a hypothesis according to which the moment of inertia of a deformed nucleus can be estimated by subtracting from the rigid-body value the moment of inertia of an inscribed sphere.

PACS numbers: 21.60. -n, 21.65. +f

1. Introduction

At last year's workshop in honour of Zdzisław Szymański (Ref. [1]) I showed the first results of adding a rotational energy to our Thomas–Fermi model of nuclei (Ref. [2]). Today I will present additional results on fission barriers, rotational gamma ray energies and moments of inertia. I will conclude with a speculation concerning an effective "inert core", which reduces the moment of inertia of a rotating nucleus below the rigid-body value.

References [1] and [2] give a description of our model, as well as a more extensive list of references. Here I will only recall that the two physical ingredients in the model are the Thomas–Fermi assumption of two fermions per h^3 of phase space volume, and the use of an effective velocity- and density-dependent Yukawa interaction between the nucleons. When angular momentum is present, all mass elements of the density distributions will be

* Presented at the XXXI Zakopane School of Physics, Zakopane, Poland, September 3–11, 1996.

assumed to rotate with the same angular velocity, except when, towards the end, the hypothesis of an "effective inert core" is being tested.

2. Fission barriers

A comprehensive survey of macroscopically calculated fission barriers was given in 1986 by A.J. Sierk within the framework of the Yukawa-plus-Exponential model of Krappe and Nix [3]. Figure 1 compares Sierk's barriers for zero angular momentum with our Thomas–Fermi calculations and with measurements. For the heaviest elements both calculations reproduce closely experiment, but then Sierk's barriers fall significantly below the Thomas–Fermi values. This continues to be the case after inclusion of angular momentum (Fig. 2). For example, in the case of a nucleus on the valley of beta-stability with atomic number $Z = 60$, the Thomas–Fermi barrier for angular momentum $L = 70$ (in units of $\hbar$) is close to 13 MeV, whereas Sierk's value is about 8.5 MeV.

Figure 3 shows the Thomas–Fermi barriers for other nuclei on the valley of stability, all with angular momentum $L = 70$. It turns out that, for given Z, fission barriers increase significantly with neutron number. Since the neutron separation energy *decreases* with increasing N, the chances of an excited compound nucleus surviving fission go up markedly when neutron-rich projectiles and targets are used in heavy-ion reactions designed to produce the highest possible angular momenta. The contour lines in Fig. 4 are labeled by the "figure of merit" Δ, defined as the difference between the fission barrier B_f and the neutron binding B_n, as calculated using the Thomas–Fermi model. The probability to emit a neutron rather than to fission is given approximately by the standard formula

$$P_n \approx \frac{1}{1 + \mathrm{e}^{-\Delta/T}}\,, \tag{1}$$

where T is a temperature. If Δ is negative the greatest danger of losing the system by fission is when T is small, say of the order 0.7 MeV, towards the end of the neutron evaporation chain. The corresponding values of P_n are indicated in Fig. 4. The dots in Fig. 4 indicate nuclei resulting from bombardments of available targets with beams of ^{48}Ca, followed by the emission of four neutrons. Relatively favorable conditions prevail for $52 \leq Z \leq 62$. An Ytterbium compound system is also a fair choice. Note that adding two neutrons can increase the survival probability from, say, 5% to 50%. Figure 4 is based on calculations of dozens of neutron binding energies and fission barriers for $L = 70$, using rigid-body moments of inertia. Since one expects actual moments of inertia to be less than rigid (see later), the absolute values of the survival probabilities in Fig. 4 may be on the optimistic side, but relative values should nevertheless be useful as a guide.

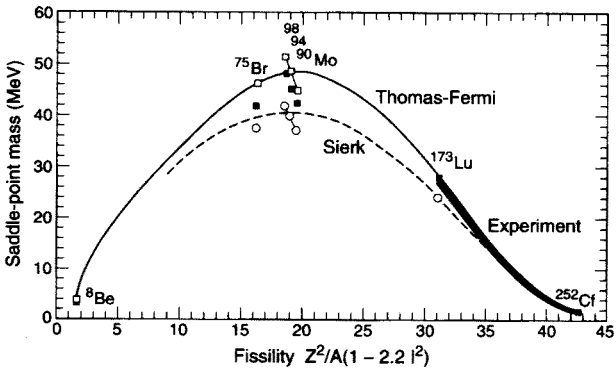

Fig. 1. Fission barriers of nonrotating nuclei against the fissility parameter $Z^2/A(1-2.2I^2)$ where $I=(N-Z)/A$. The shaded band and the solid squares refer to measurements. The dashed curve refers to nuclei along Green's valley of stability, given by $N-Z=0.4A^2/(200+A)$, and the open circles to individual nuclei, as deduced from Sierk's survey [3]. The solid curve and open squares represent the Thomas–Fermi results.

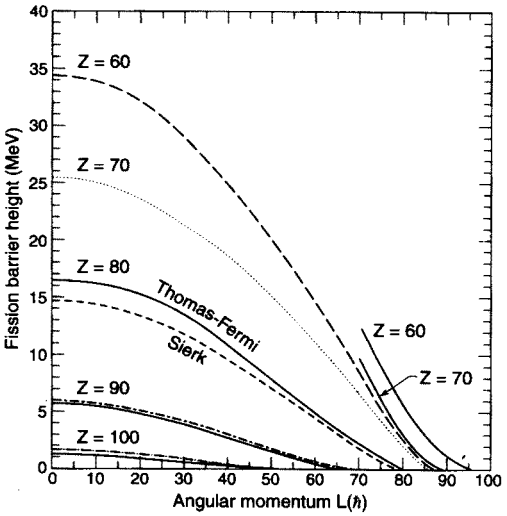

Fig. 2. The dependence on angular momentum of fission barriers for nuclei on the valley of stability. Solid curves are the Thomas–Fermi results, the broken curves refer to Sierk's barriers.

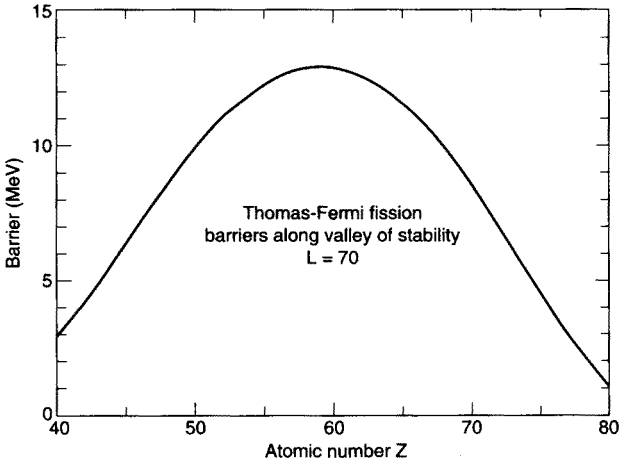

Fig. 3. Thomas–Fermi fission barriers for nuclei along the valley of stability with angular momentum $L = 70$.

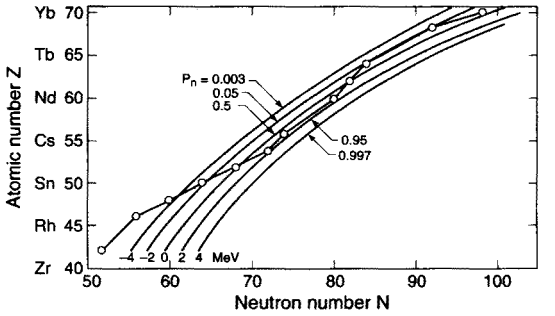

Fig. 4. Contour plots of Δ, the difference between the fission barrier and the neutron binding energy, as calculated using the Thomas–Fermi model for nuclei with angular momentum $L = 70$. The contours are labeled by Δ, as well as by the probability P_n to emit a neutron (*i.e.*, to survive fission) for a temperature $T = 0.7$MeV, typical of the end of a neutron evaporation chain.

Figure 5 shows the deformation energies of ^{194}Hg with $L = 0, 10, 20, 30, 40, 50, 60, 70$. Each curve is the result of some 30 constrained Thomas–Fermi calculations of the binding energy, the constraint being the quadrupole moment of the rotating nucleus, taken with respect to an axis at right angles to the rotation axis. The difference in energy between the maximum and minimum for each curve is the Thomas–Fermi fission barrier. Also shown as crosses are the measured binding energy of the ground state of ^{194}Hg and of the $L = 10, 20, 30, 40, 50$ rotational states of the "SD-1" superdeformed band, whose quadrupole moment is $Q_0 = 17.2$b. The difference between the top of the calculated barrier and the *measured* rotational state gives

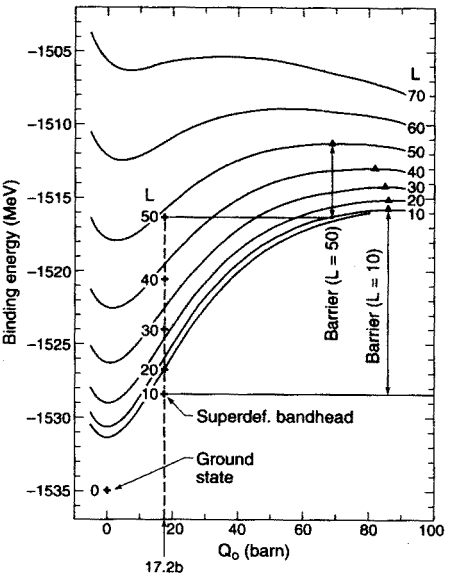

Fig. 5. The binding (or deformation) energies of ^{194}Hg for different angular momenta, plotted against Q_0, the quadrupole moment with respect to an axis at right angles to the axis of rotation. Triangles locate the saddle-point configurations. Crosses refer to the measured binding energy of the ground state and to the $L = 10, 20, 30, 40, 50$ states of the SD-1 superdeformed band in ^{194}Hg, whose absolute energies were determined recently. The energy differences between corresponding triangles and crosses provide estimates of the fission barriers in their dependence on angular momentum.

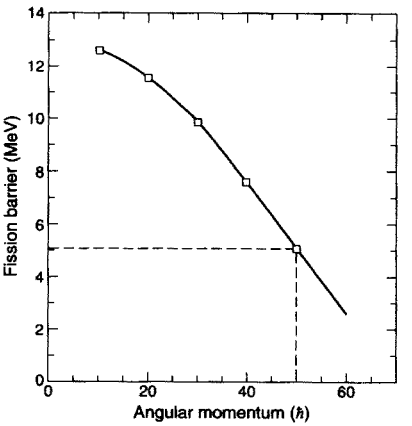

Fig. 6. The fission barriers for the SD-1 superdeformed band in ^{194}Hg, as deduced from Fig. 5. The state with the highest observed angular momentum, $L = 50$, is thus estimated to have a 5 MeV fission barrier.

an improved estimate of the corresponding fission barrier, subject only to the uncertainty of the calculated saddle-point energy. (There are reasons to believe that macroscopically calculated saddle-point energies are relatively accurate — see the "topographic theorem" of Ref. [2].) Figure 6 shows the fission barriers of the SD-1 band in ^{194}Hg calculated in this way. Figure 7 shows the saddle-point shape of ^{194}Hg at zero angular momentum.

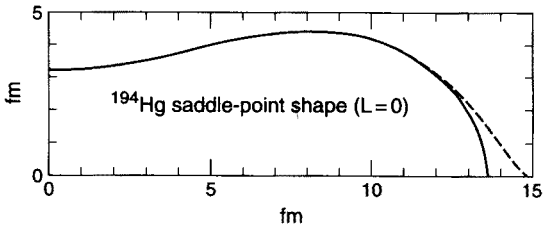

Fig. 7. The saddle-point shape of ^{194}Hg with $L = 0$. The solid curve gives (except towards the tip) the effective sharp radius of density slices taken at right angles to the major axis of the axially symmetric density distribution. The dashed curve extends beyond the effective location of the major axis because of the surface diffuseness

3. Rotational bands and moments of inertia

Reading off the sequence of calculated energies in Fig. 5 at the measured quadrupole moment $Q_0 = 17.2$ b, one can deduce the predicted Thomas–Fermi gamma-ray energies in the superdeformed band of ^{194} Hg at this quadrupole moment. The result is compared with measurements in Fig. 8. The calculated energies are lower, implying that the rigid-body moments of inertia used in the calculation are too high. The deduced ratio $J_{\mathrm{exp}}/J_{\mathrm{rigid}}$ is plotted against the square of the rotation frequency $(\hbar\omega)^2$ in Fig. 9, along

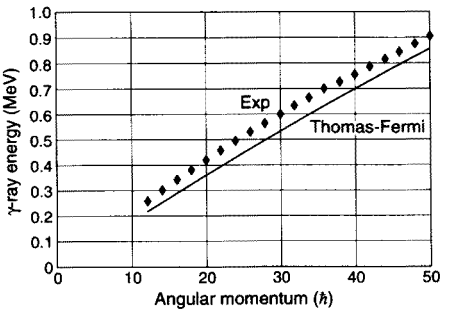

Fig. 8. The γ-ray energies as functions of the angular momentum for the superdeformed band in ^{194}Hg, as found experimentally (diamonds) and as calculated using the Thomas–Fermi model.

with similar ratios for the SD-1 superdeformed bands in ^{152}Dy and ^{132}Ce, as well as for the ground-state rotational bands for ^{172}Hf and ^{238}U. The resulting plots show the familiar trends, often interpretable quantitatively in terms of spin alignment and the quenching of pairing interactions.

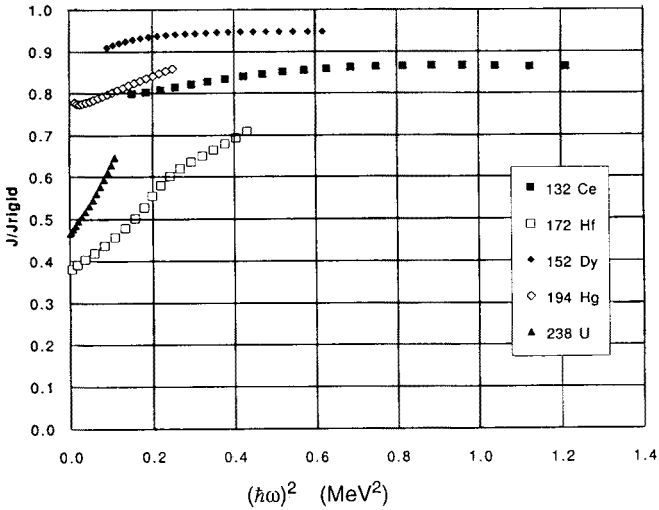

Fig. 9. The ratio of the measured moment of inertia to the Thomas–Fermi rigid-body value, as deduced from plots similar to Fig. 8, in the case of ground-state rotational bands in ^{238}U and ^{172}Hf, and superdeformed SD-1 bands in ^{194}Hg, ^{152}Dy and ^{132}Ce.

We used Fig. 9 to test a speculation that the above effects might correlate with a simple geometrical property of the rotating nuclei. Figure 10 illustrates the idea: a rotating deformed diffuse potential well perturbs the particles it contains only in a region outside a core whose radius is approximately equal to the minor axis of the shape in question; inside this core the potential is virtually time-independent. It is true that for strictly independent particles in a rotating, deformed potential this makes no difference and (in the Thomas–Fermi approximation) the response of such a gas of particles to rotation is always that of a rigid-body. But to the extent that residual interactions hamper such an optimum alignment of the particles' angular momenta, the resulting decrease of the moment of inertia might well be correlated with the region in space where the rotation potential is ineffective in breaking up the pairing correlations. However that may be, Fig. 9 was used to calculate, for each nucleus, the radius of an effective inert core such that, after its excision, the rigid moment of inertia of the remainder matches the measured values. Will the radii thus obtained be at all comparable with the minor axes of the rotating shapes? Figure 11 shows

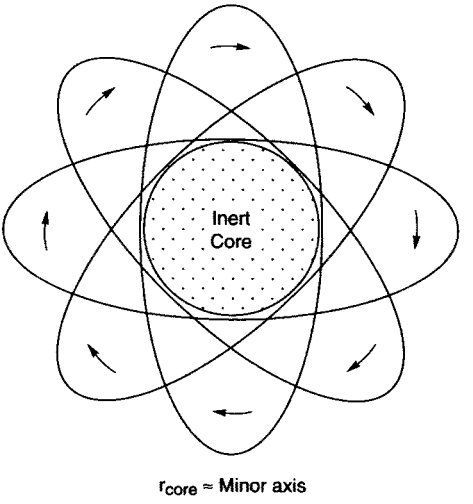

Fig. 10. A rotating, deformed, slightly diffuse potential well is characterized by a core where the potential exhibits no time dependence. Is there a correlation between the size of such a core and the deviation of the observed moment of inertia from the rigid-body value?

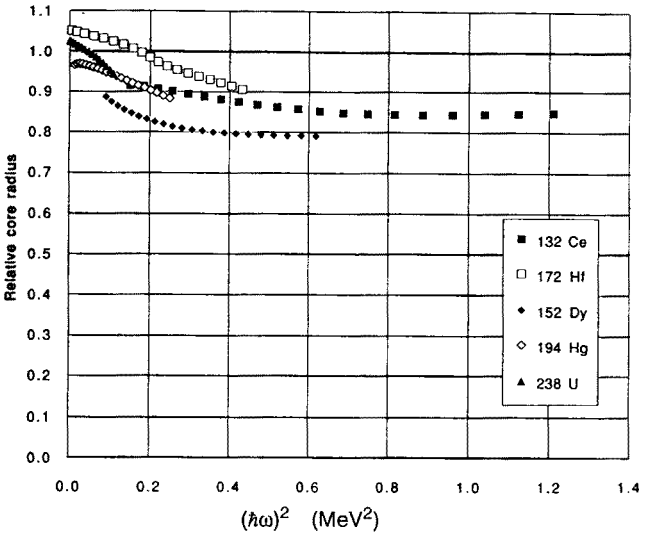

Fig. 11. The deviation of the moment of inertia from the rigid-body limit in Fig. 9 was translated into an effective inert core radius, *i.e.*, the radius of a core whose moment of inertia, when subtracted from the rigid-body value, would ensure agreement with measurement. The resulting radii, in units of the relevant mean transverse axis, are plotted as functions of the square of the rotational frequency ω.

the radii of the excised cores in units of the corresponding minor axes for the five nuclei in question (actually the mean of the two transverse minor axes of the triaxial shapes). A more or less universal trend, not very different from unity is, indeed, suggested. (The experimental moments of inertia in Figs. 9 and 11 were deduced by dividing the square of the angular momentum by twice the rotational energy $E_{\mathrm{ROT}}(L)$; one might call this the "geometric" moment of inertia $J^{(0)}$ to distinguish it from the kinematic and dynamic moments of inertia $J^{(1)}$ and $J^{(2)}$. In the case of superdeformed rotational bands, which do not start at $L = 0$, the absolute value of $E_{\mathrm{ROT}}(L)$ can only be estimated by extrapolating $E_{\mathrm{ROT}}(L)$ down to zero angular momentum. This introduces some uncertaintity in the deduced values of $J^{(0)}$ over and above the uncertaintity resulting from the inaccuracy in the estimated angular momenta of the superdeformed bandheads.)

4. Ubiquitous superdeformations?

Whether there is a physical basis for assuming an effective inert core remains to be seen. However, if it is really true that the moment of inertia of a rotating nucleus may be estimated by cutting out an effective core corresponding to an inscribed sphere, two obvious, but otherwise qualitative predictions can be made more quantitative. Figure 12 shows the calculated deformation energies of ^{135}Nd with $L = 60$, resulting from assuming an inert core whose radius is 0, 0.8, 0.9, or 1.0 in units of the mean transverse axis of the rotating Thomas–Fermi nucleus. In the first case the calculated Thomas–Fermi ground state is a slightly oblate shape with Q_0 close to zero. But if a core is cut out, the moment of inertia becomes small as the shape approaches axial symmetry for small Q_0, and the rotational energy grows correspondingly. There results a tendency to avoid small Q_0 values, and equilibrium deformations with quadrupole moments in the range 10–20 b can be expected. Thus a new type of ubiquitous superdeformed nuclei is predicted, the superdeformation not being governed by the presence of shell effects for special neutron and proton numbers. Figure 13 shows how the quadrupole moments of such superdeformed shapes would grow with increasing L for three different assumptions about the size of the inert core. Experimentally, one might look for evidence of such superdeformations in the lifetimes of unresolved continuum gamma rays.

The second prediction implied by Fig. 12 is a significant lowering of fission barriers with increasing angular momentum. This is because the relative moment of inertia of an inscribed sphere for a necked-in-saddle-point shape is almost negligible, so that the saddle-point energy stays almost unaffected, whilst the energy of the equilibrium shape is pushed up by the increased rotational energy caused by the decreased moment of inertia.

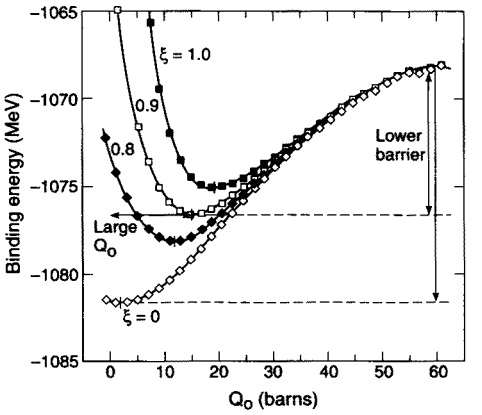

Fig. 12. An illustration in the case of ^{135}Nd, rotating with $L = 60$, of the consequences of assuming that the moment of inertia can be estimated by cutting out an effective inert core (with radius equal to 0.8, 0.9, or 1.0 times the mean transverse axis). When such a core is excised, the resulting deformation energies predict large equilibrium deformations and reduced fission barriers.

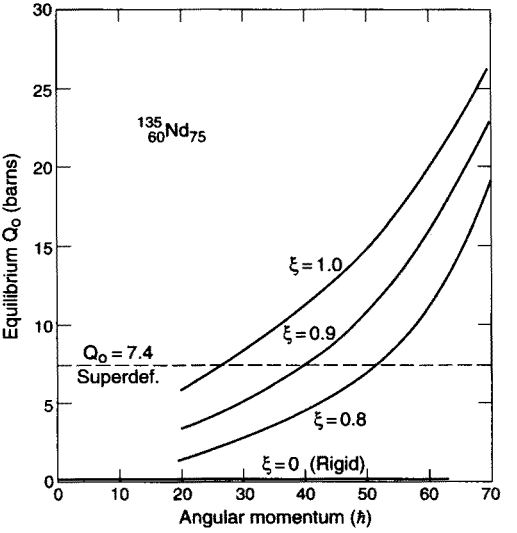

Fig. 13. The equilibrium deformations, as measured by the quadrupole moment Q_0, are plotted as a function of angular momentum for ^{135}Nd, for three values of ξ, the radius of the excised core relative to the mean transverse axis.

Systematic measurements of the angular momentum dependence of fission barriers, as well as the above mentioned measurements of the lifetimes of continuum gamma rays may throw light on the hypothesis of an effective inert core.

We would like to thank Frank and Marie-Agnes Stephens, Paul Fallon and Stefan Frauendorf for many enlightening discussions concerning rotating nuclei, and Gordon Wozniak and Luciano Moretto for sharing their data on fission barriers. This work was supported by the Director, Office of Energy Research, Division of Nuclear Physics of the Office of High Energy and Nuclear Physics of the U.S. Department of Energy under Contract No. DE-AC03-76SF00098.

REFERENCES

[1] W.D. Myers, W.J. Świątecki, *Acta Phys. Pol.* **B27**, 99 (1996).

[2] W.D. Myers, W.J. Świątecki, *Nucl. Phys.* **A601**, 141 (1996).

[3] A.J. Sierk, *Phys. Rev.* **C33**, 2039 (1986).